

**Supporting information for:**

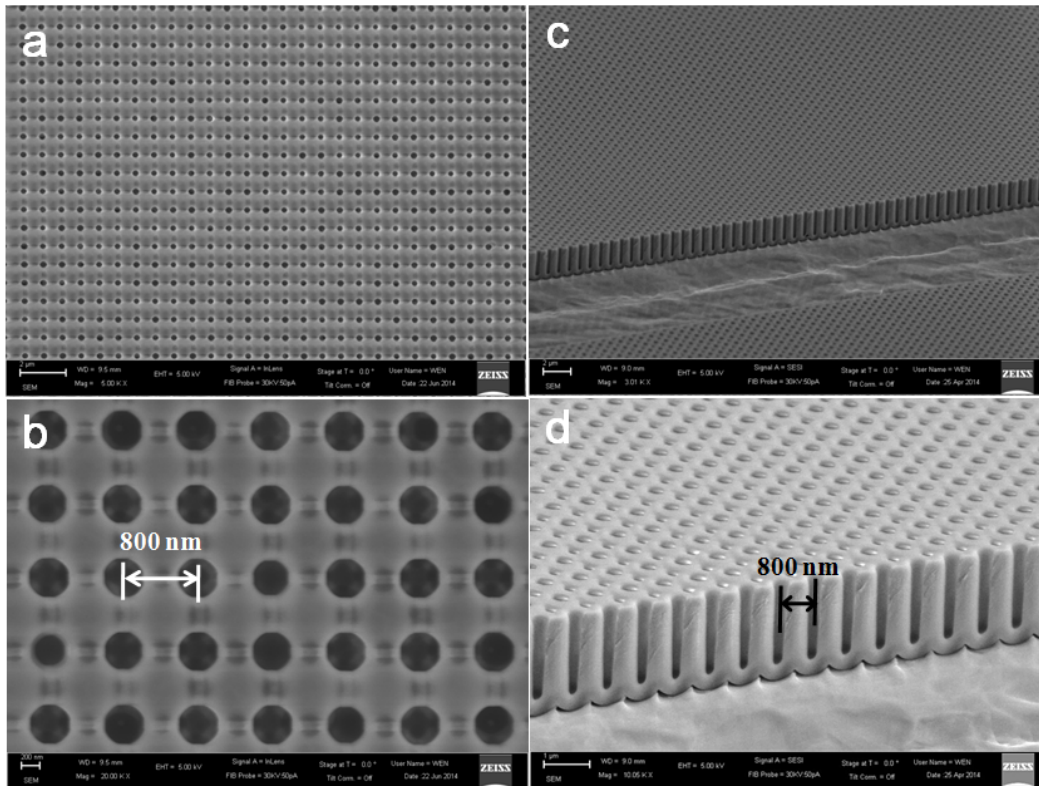
**Large-scale Highly Ordered Sb Nanorod Arrays Anode with High  
Capacity and Rate Capability for Sodium-Ion Batteries**

*Liying Liang, Yang Xu, Chengliang Wang, Liaoyong Wen, Yaoguo Fang, Yan Mi, Min Zhou,  
Huaping Zhao, and Yong Lei\**

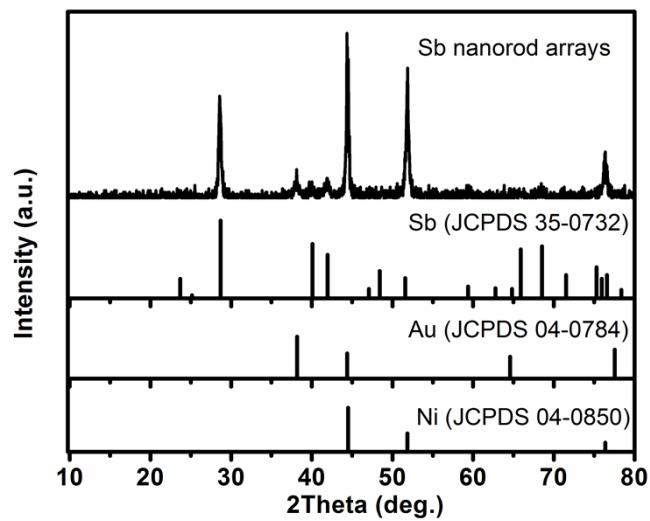
Institute for Physics and IMN MacroNano<sup>®</sup>, Technical University of Ilmenau, Ilmenau 98693,  
Germany

Fax: +49(0)3677 69-3746; Tel: +49(0)3677 69-3748;

E-mail: [yong.lei@tu-ilmenau.de](mailto:yong.lei@tu-ilmenau.de)



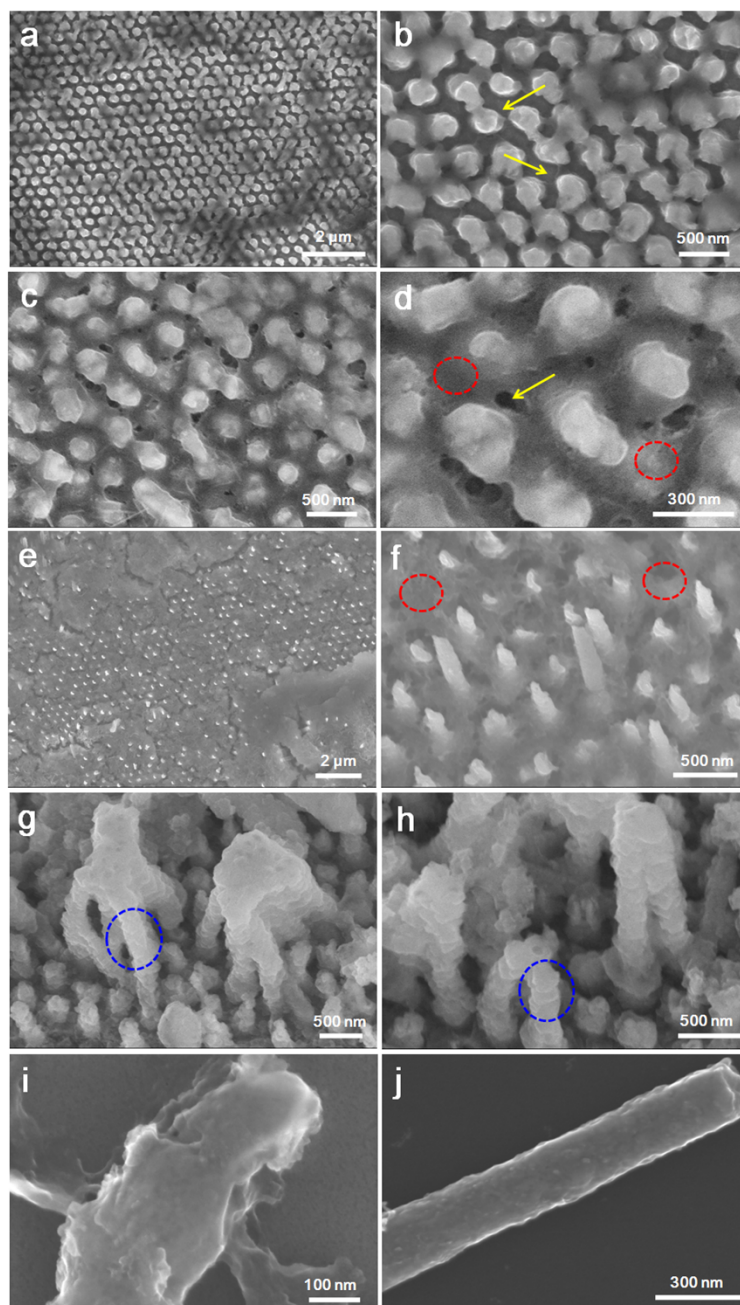
**Fig. S1** SEM images of nanoimprinted AAO template with cell size of 800 nm.



**Fig. S2** XRD pattern of Sb nanorod arrays on Au/Ni substrate.

**Table S1** Cycling performance comparison of the as-prepared Sb nanorod arrays with previously reported Sb-based anodes.

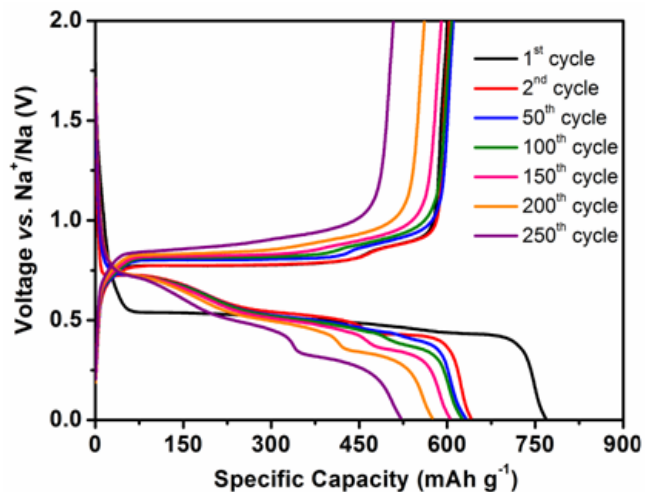
Materials	Current density/A g <sup>-1</sup>	Cycles	Retention	Last cycle capacity /mAh g <sup>-1</sup>
Monodisperse Sb Nanocrystals <sup>1</sup>	0.66	100	> 90%	~580
SnSb-porous carbon nanofibers <sup>2</sup>	0.1	205	> 90%	~345
Bulk Sb <sup>3</sup>	0.33	160	> 90%	~576
rGO/Sb <sub>2</sub> S <sub>3</sub> <sup>4</sup>	0.05	50	~90%	~620
Sn-Ge-Sb thin film alloys <sup>5</sup>	0.425	50	~73%	~662
Sb-C nanofibers <sup>6</sup>	0.2	400	> 90%	~450
Sb/C fibers <sup>7</sup>	0.1	300	~83%	~350
	0.5	140	> 90%	~571
S-Sb NRs	0.2	100	> 90%	~620
(this work)		250	~84%	~521



**Fig. S3** SEM images of S-Sb NRs after different charge/discharge cycles. a) and b) after the 100th cycle. c) and d) after the 150th cycle. e) and f) after the 200th cycle. g-i) after the 250th cycle. j) before cycling.

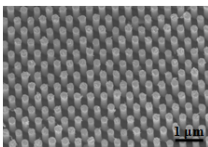
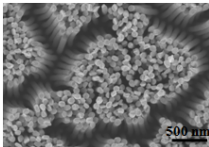
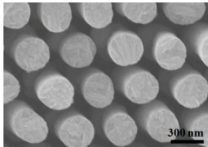
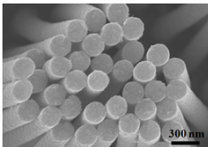
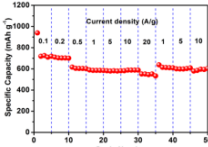
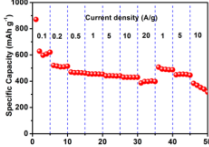
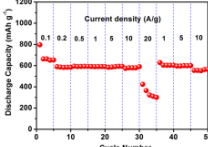
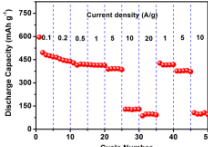
Although the cycle life was prolonged at a relatively low current density, there still should have some space for further improvement. Therefore, we analyzed the fading mechanism by

investigating the structure change during cycling and provided the directions for further improvement. Fig. S3 shows the SEM images of Sb nanorod arrays anode after various cycles at a current density of  $0.2 \text{ A g}^{-1}$ . The highly ordered and vertically well-aligned feature with clear interval spacing still was maintained after 100 cycles (Fig. 2c and Fig. S4). Meanwhile, a thin layer of SEI film around Sb nanorod can be observed. The SEI film gradually became thicker upon cycling, as shown in Fig. S3c and d, which is attributed to continuous formation of new SEI film deriving from large volume changes of Sb (390%) in repeated Na alloying/dealloying processes. After 150 cycles, the SEI film (as indicated by red circle) has filled the part of interval spacings, whereas there still had enough spacing for electrolyte infiltration (as shown by yellow arrow), which is beneficial for cycling stability. After 200 cycles (Fig. S3e and f), most of interval spacings had been filled by the thicker SEI film, leading to slow ions diffusion, then followed by the slight decay of capacity (as shown in Fig. 2c). Except the adverse effect of SEI film, as far as we know, the large volume change of Sb is another factor for the capacity decay, which is also considered to be the major reason for capacity decay of bare alloy-based materials.<sup>5</sup> Before 200 cycles, due to the chemical and mechanical robustness of our arrays electrode, the Sb nanorod maintained its integrity, resulting in stable cycling performance. However, with longer cycling, this huge volume change caused the pulverization, and then the surface of nanorod became cracked, as indicated by the blue circles in Fig. S3g and h. We scratched Sb nanorods off the current collector in order to observe the single nanorod, as shown in Fig. S3i. The magnified SEM image displays the clear cracks on the surface of Sb nanorod compared to the pristine Sb nanorod before cycling (Fig. S3j) which shows the complete nanorod structure without any cracks. The increasing volume change damaged the electrode integrity, resulting in a loss of contact between active material and current collector. As a consequence, upon cycling, more capacity fading was observed. The decay can also be accordingly reflected on charge/discharge profiles at various cycles (Fig. S4). At high rates, the phenomenon of volume changes would be more obvious, thus accelerating the capacity decay. Therefore, Sb nanorod arrays anode showed a shorter cycle life at the larger current density of  $0.5 \text{ A g}^{-1}$  than at  $0.2 \text{ A g}^{-1}$  (Fig. 2c).



**Fig. S4** Galvanostatic charge/discharge voltage profiles of S-Sb NRs at a current density of 0.2 A g<sup>-1</sup>.

**Table S2** Structure and electrochemical performance comparison of four different Sb nanorod arrays.

Name	S-Sb NRs	A-Sb NRs	S-2-Sb NRs	A-2-Sb NRs
Cell Size	400	110	400	400
Diameter/nm	210	70	300	210
Length/ $\mu\text{m}$	1.5	1.5	1.5	6.0
Interval Spacing	190	Limited	100	Limited
Aspect Ratio (L vs. D)	7.14	21.43	5	28.57
Well-aligned	√	/	√	/
Attached	/	√	/	√
Morphology				
Electrochemical Performance				

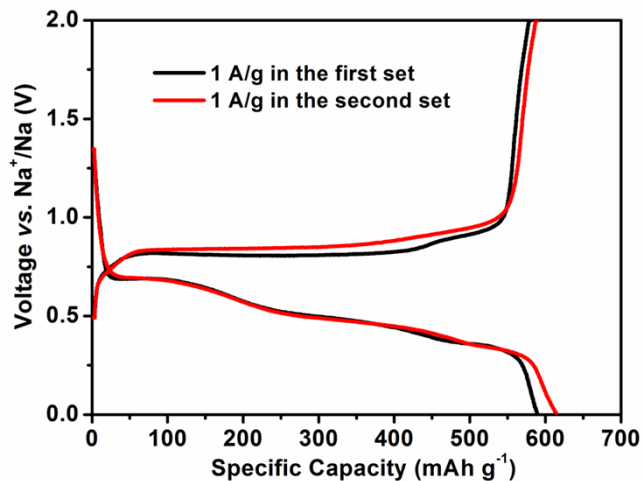


**Fig. S5** Galvanostatic charge/discharge voltage profiles of S-Sb NRs at the current density of 1 A g<sup>-1</sup> in different rate sets.

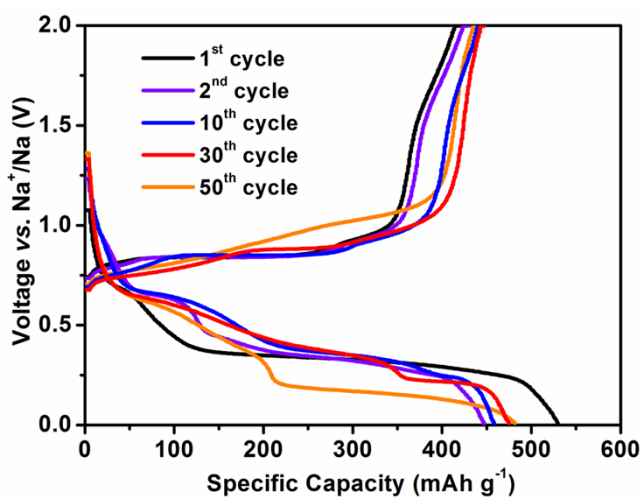


**Fig. S6** Galvanostatic charge/discharge voltage profiles of A-Sb NRs electrode at a current density of 1 A g<sup>-1</sup>.

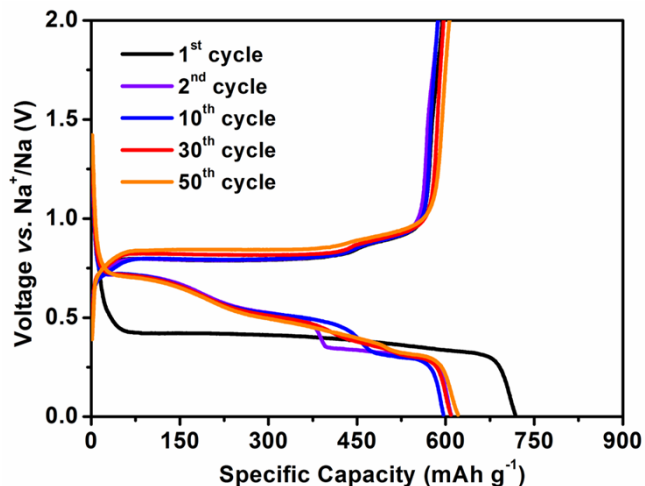


**Fig. S7** Galvanostatic charge/discharge voltage profiles of S-Sb NRs electrode at a current density of  $1 \text{ A g}^{-1}$ .

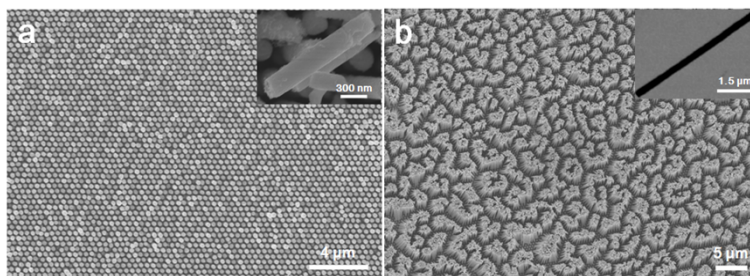


**Fig. S8** SEM images of a) S-2-Sb NRs and b) A-2-Sb NRs. The single Sb nanorod was observed by scratching Sb arrays off the Ni/Au substrate.

In the manuscript, the comparison between S-Sb-NRs and A-Sb-NRs has shown the effect of the spacing between rods on the electrochemical performances. The difference of spacing was realized by using the templates with different cell size, i.e., 400 nm for S-Sb-NRs and 110 nm for A-Sb-NRs. To further demonstrate the effect of spacing between rods, another reference sample (S-2-Sb-NRs) with the same cell size of 400 nm was fabricated. By changing the diameter of the rods from 190 to 300 nm, the spacing between rods has been changed from 210 to 100 nm. SEM images can be found in Fig. S8a. The electrochemical performance of S-2-Sb NRs (Table S2)



displays the large and stable capacities from the current density of 0.1 to 10 A g<sup>-1</sup>, due to its highly ordered alignment. However, a capacity decay was observed at 20 A g<sup>-1</sup>, supposed to that the interval spacing of 100 nm is not enough to accommodate the huge volume changes of Sb nanorod arrays at such a large current density. It is worth noting that, the above-mentioned results also reflect the effect of the diameter since the two samples, S-Sb-NRs and S-2-Sb-NRs, possess identical structural parameters except for the diameter.

To demonstrate the effect of aspect ratio (L vs. D), a reference sample (A-2-Sb-NRs) was fabricated. The sample has the same structural parameters with S-Sb-NRs except for the length which has been increased to 6.0 μm (Fig. S8b), giving rise to an aspect ratio of 28.57 (vs. 7.14 for S-Sb-NRs). A-2-Sb NRs displayed lower capacity than S-Sb NRs, and serious capacity decay at the large current densities of 10 and 20 A g<sup>-1</sup>. Because it is difficult for electrolyte transferring into the internal region of attached arrays, in particular at large rates, and very limited interval spacing is adverse to the stress strain.

On the basis of the above results, it is reasonable to conclude that, although the aspect ratio has effects on the electrochemical performance of Sb nanorod arrays to some extent, highly ordered alignment and large enough interval spacing are determinate factors. The above results are consistent with those in the manuscript where highly ordered arrays with large interval spacing are largely beneficial to the electrochemical performance.

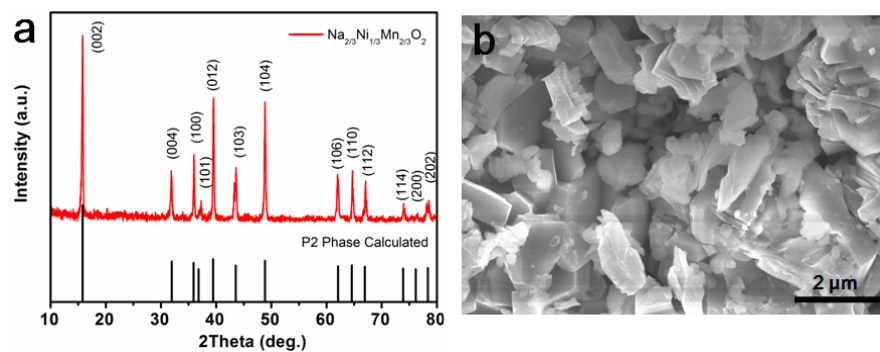


**Fig. S9** a) XRD pattern and b) SEM image of layered P2- $\text{Na}_{2/3}\text{Ni}_{1/3}\text{Mn}_{2/3}\text{O}_2$ .

The crystal structure of the as-prepared material was studied by XRD as shown in Fig. S9a. The XRD pattern shows a layered structure belonging to the hexagonal P63/mmc space group, indexed as a P2-type structure.<sup>8-10</sup> The typical layered morphology is also observed in Fig. S9b, in which a series of planes constitute single particles with an average size of 1~2  $\mu\text{m}$ . Therefore, layered P2- $\text{Na}_{2/3}\text{Ni}_{1/3}\text{Mn}_{2/3}\text{O}_2$  has been successfully synthesized.

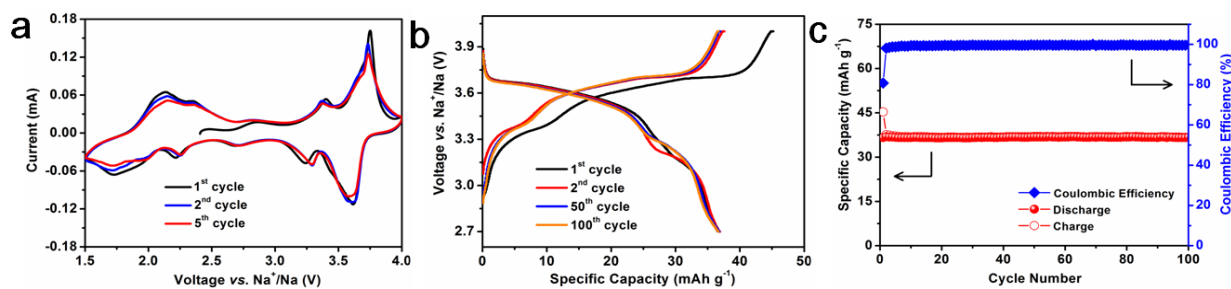


**Fig. S10** Electrochemical performance of layered P2- $\text{Na}_{2/3}\text{Ni}_{1/3}\text{Mn}_{2/3}\text{O}_2$  in a Na cell. a) Cyclic voltammetry at a scan rate of  $0.1 \text{ mV s}^{-1}$  between 1.5 to 4.0 V (vs.  $\text{Na}^+/\text{Na}$ ). b) Galvanostatic charge/discharge voltage profiles in different cycles, and c) cycling performance at a current density of  $30 \text{ mA g}^{-1}$  between 2.7 to 4.0 V (vs.  $\text{Na}^+/\text{Na}$ ).

The electrochemical performance of as-prepared P2- $\text{Na}_{2/3}\text{Ni}_{1/3}\text{Mn}_{2/3}\text{O}_2$  in a half cell was investigated in the electrolyte of 1 M  $\text{NaClO}_4$  in EC: PC (1:1 by volume) with the addition of 5% FEC. Fig. S10a displays its CV profiles of the first five cycles, which have similar shapes with

reported P2-Na<sub>2/3</sub>Ni<sub>1/3</sub>Mn<sub>2/3</sub>O<sub>2</sub> cathodes.<sup>8-10</sup> Galvanostatic charge/discharge curves of P2-Na<sub>2/3</sub>Ni<sub>1/3</sub>Mn<sub>2/3</sub>O<sub>2</sub> at a current density of 30 mA g<sup>-1</sup> were also conducted, as shown in Fig. S10b. The cut off potential was set to 2.7-4.0 V (vs. Na<sup>+</sup>/Na), because it was reported that this range can ensure the reversibility of P2-Na<sub>2/3</sub>Ni<sub>1/3</sub>Mn<sub>2/3</sub>O<sub>2</sub> cathode.<sup>4</sup> It can be seen that P2-Na<sub>2/3</sub>Ni<sub>1/3</sub>Mn<sub>2/3</sub>O<sub>2</sub> showed typical and reversible voltage profiles, which are consistent with the characteristic peaks on the CV curves in Fig. S10a. A reversible capacity for this cathode of 38 mAh g<sup>-1</sup> is obtained between 2.7-4.0 V at a current density of 30 mA g<sup>-1</sup>. Fig. S10c shows its cycling performance, in which P2-Na<sub>2/3</sub>Ni<sub>1/3</sub>Mn<sub>2/3</sub>O<sub>2</sub> maintained superior cycling stability (100% capacity retention over 100 cycles) and high CE of around 99.5%.

## References

1. M. He, K. Kravchuk, M. Walter and M. V. Kovalenko, *Nano Lett.*, 2014, **14**, 1255-1262.
2. L. Ji, M. Gu, Y. Shao, X. Li, M. H. Engelhard, B. W. Arey, W. Wang, Z. Nie, J. Xiao, C. Wang, J. G. Zhang and J. Liu, *Adv. Mater.*, 2014, **26**, 2901-2908.
3. A. Darwiche, C. Marino, M. T. Sougrati, B. Fraisse, L. Stievano and L. Monconduit, *J. Am. Chem. Soc.*, 2012, **134**, 20805-20811.
4. D. Y. W. Yu, P. V. Prikhodchenko, C. W. Mason, S. K. Batabyal, J. Gun, S. Sladkevich, A. G. Medvedev and O. Lev, *Nat. Commun.*, 2013, **4**, 2922-2928.
5. B. Farbod, K. Cui, W. P. Kalisvaart, M. Kupsta, B. Zahiri, A. Kohandehghan, E. M. Lotfabad, Z. Li, E. J. Lubber and D. Mitlin, *ACS Nano*, 2014, **8**, 4415-4429.
6. L. Wu, X. Hu, J. Qian, F. Pei, F. Wu, R. Mao, X. Ai, H. Yang and Y. Cao, *Energy Environ. Sci.*, 2013, **7**, 323-328.
7. Y. Zhu, X. Han, Y. Xu, Y. Liu, S. Zheng, K. Xu, L. Hu and C. Wang, *ACS Nano*, 2013, **7**, 6378-6386.
8. Y. Wen, B. Wang, G. Zeng, K. Nogita, D. Ye and L. Wang, *Chem. Asian. J.*, 2015, **10**, 661-666.
9. D. H. Lee, J. Xu and Y. S. Meng, *Phys. Chem. Chem. Phys.*, 2013, **15**, 3304-3312.
10. Z. Lu and J. R. Dahn, *J. Electrochem. Soc.*, 2001, **148**, A1225-A1229.